IEEE Access
Multidisciplinary | Rapid Review | Open Access Journal

Received May 3, 2022, accepted May 19, 2022, date of publication June 10, 2022, date of current version June 20, 2022.

Digital Object Identifier 10.1109/ACCESS.2022.3182095

Design and Experimental Study of Ultrasonic Vibration Feeding Device With Double Symmetrical Structure

JIAN ZHANG AND XIAOZHU WANG
Yingkou Institute of Technology, Yingkou, Liaoning 115014, China

Corresponding author: Xiaozhu Wang (330608566@qq.com)

This work was supported in part by the Liaoning Natural Science Foundation Joint Fund Project under Grant 2021-YKLH-07 and Grant 2020-YKLH-28, in part by the Liaoning Provincial Department of Education Funding for Scientific Research under Grant L2020007, and in part by the Program for Excellent Talents of Science and Technology in Yingkou Institute of Technology under Grant RC202003.

ABSTRACT In view of the limitations of traditional feeder driving mode in bulk material conveying, a new scheme of ultrasonic vibration feeding device with double symmetrical axis structure is proposed based on the existing traveling wave ultrasonic material conveying device. The outer sides of the upper and lower straight beam sections of the symmetrical conveying vibrator contain convex tooth structures, and piezoelectric ceramic sheets are pasted on the inner side; Based on the piezoelectric driving principle and the quarter wavelength principle, the conveying vibrator is dynamically designed, the influence of geometric size on the vibrator frequency is analyzed, the bending vibration mode of the vibrator is selected as 18 order, and the principle prototype of ultrasonic vibration feeding device is made. The resonant frequency difference measured in the experiment is close to that obtained by theoretical analysis, Moreover, the amplitude distribution of the conveying vibrator tooth surface is basically consistent with the finite element analysis results, and the influence law of material types on the conveying rate is compared and analyzed. The test results show that the ultrasonic vibration feeding device has a certain conveying capacity, the conveying rate is adjustable in a certain range, has high control accuracy, and meets the engineering application.

INDEX TERMS Vibratory feeding device, symmetric structure, ring type piezoelectric vibrator, traveling wave, ultrasonic vibration.

I. INTRODUCTION

Ultrasonic material conveying device is a new type of ultrasonic driver derived from ultrasonic motor, which is completely different from the traditional material conveying device in principle[1]. Compare with the traditional conveying device, it has no shaft, rod and other mechanical transmission parts, simple structure and easy to manufacture [2]; The conveying rate can be controlled by changing any parameter of the driving signal (such as voltage, frequency, amplitude, etc.) [3], so there are many control parameters and good controllability [4]. And it don't produce interference electromagnetic field and is not affected by electromagnetic interference signal [5]; it has the characteristics of quiet, no noise and fast response [6].

The associate editor coordinating the review of this manuscript and approving it for publication was Kan Liu.

When the traveling wave ultrasonic vibration feeding device working, the contact pressure and contact deformation are generated between the conveying vibrator and the material through the self-weight of the material [7]. Because of the longitudinal displacement at the contact, the material is out of contact with the particle at the peak position on the conveying vibrator, The transverse displacement at the contact pushes the material forward in a single direction by friction [8]. It can be seen that the conveying vibrator is the major component of the ultrasonic vibration feeding device [9]. In order to design a high-performance ultrasonic vibration feeding device, only by clarifying the dynamic characteristics of the conveying vibrator [10].

The structure of the traditional long ring vibrator is shown in Figure 1. Because the vibrator of this structure is designed with convex tooth structure on the outside of the upper straight beam section, and the ceramic sheet is pasted on the outside of the lower straight beam section, which causes the

upper and lower parts of the vibrator structure are strictly asymmetric, it is difficult to find the optimal mode in the finite element analysis, and with the further widening of the width dimension, it is easy to have obvious bending deformation in the width direction [11]. Therefore, the industrialization of ultrasonic material conveying technology depends on the in-depth discussion of ultrasonic driving principle [12].

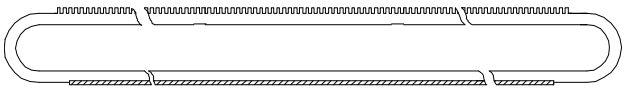

FIGURE 1. Structure of traditional long ring vibrator.

In view of the problems existing in the traditional long ring ultrasonic material conveying device, in this paper, an ultrasonic vibration feeding device with symmetrical structure is designed. The conveying vibrator with double symmetrical axis structure can well solve the above problems and has better conveying performance for different materials.

II. THEORETICAL BASIS OF ULTRASONIC VIBRATION FEEDING DEVICE DESIGN

In this paper, a symmetrical structure is introduced base on the traditional long ring vibrator structure. The service life of the symmetrical structure vibrator is twice that of the traditional long ring vibrator, Since any one of the upper and lower conveying surfaces is worn for a long time, and then the conveying performance of the conveying device is reduced, The other conveying surface is used to make the conveying vibrator continue to work.

At the same time, in order to improve the conveying rate of the vibrator (amplifying the surface amplitude of the vibrator), a convex tooth structure is designed outside the upper and lower straight beam sections of the vibrator elastomer. Since the condition for synthesizing in-plane bending traveling waves is to excite two-phase approximately orthogonal in-plane bending vibration modes of the same order in the vibrator [13], it is required to find two-phase approximately orthogonal in-plane bending modes of the same order in the theoretical analysis.

Considering that in order to reduce the hollow structure, the pasting difficulty of piezoelectric ceramic sheet is increased [14], so that the pasting position of piezoelectric ceramic sheet only is located on the inner side of the upper and lower straight beam sections. Therefore, the prototype of the designed symmetrical structure vibrator is shown in Figure 2.

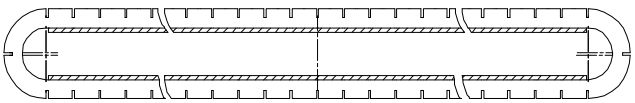

FIGURE 2. Prototype of symmetrical feeding vibrator.

The section line is piezoelectric ceramic sheet in Figure 2. Compare with Figure 1 and Figure 2, it is found that the number of convex teeth in the upper and lower straight beam sections of the symmetrical structure vibrator is reduced and the tooth width is increased. Because the wire cutting technology is used in the later processing of the vibrator [15], so as to achieve higher cost performance [16].

A. IN-PLANE VIBRATION ANALYSIS OF CIRCULAR RING STRUCTURE

The long ring structure evolves from the ring [17], Referring to the bending vibration of the ring in its torus, the ring structure is shown in Figure 3 [18].

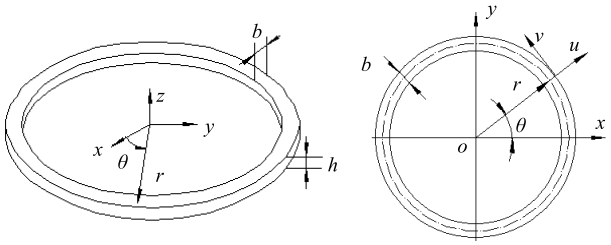

FIGURE 3. Structure schematic of a circular ring.

In Figure 3, h is the thickness of the ring and b is the radial width of the ring.

It is assumed that the plane of the ring (x-y plane) is the symmetrical plane of each cross-section [19], and the cross-sectional dimension of the ring is very small compares with its centerline radius r [20], From radial displacement (positive outward) u and tangential displacement (increasing direction of θ is positive) v, and the unit elongation at any point on the ring center line is

$$e = \frac{u}{r} + \frac{\partial v}{r\partial\theta} \tag{1}$$

In the Equation (1): The angle at one point on the ring is θ.

The expression for the change of curvature is

$$\frac{1}{r+\Delta r} - \frac{1}{r} = -\frac{\partial^2 u}{r^2\partial\theta^2} - \frac{u}{r^2} \tag{2}$$

In the case of bending vibration in the ring plane, the radial displacement u is expanded into trigonometric series

$$u = \sum_{i=1}^{\infty} [a_i \cos(i\theta) + b_i \sin(i\theta)] \tag{3}$$

In the Equation (3): the coefficients a_i and b_i are functions of time.

And it is defined that the number i for circumferential wavelengths of ring bending deformation is the order of vibration mode.

Considering the bending vibration without expansion, Set $e = 0$, which is obtained from equation (1)

$$u = -\frac{\partial v}{\partial\theta} \tag{4}$$

Substitute Equation (3) into Equation (4) and integrated to obtain

$$v = \sum_{i=1}^{\infty} [-\frac{a_i}{i} \sin(i\theta) + \frac{b_i}{i} \cos(i\theta)] \tag{5}$$

The bending moment of any cross section on the ring is

$$M = -\frac{EI}{r^2}(\frac{\partial^2 u}{\partial \theta^2} + u) \tag{6}$$

In the Equation (6): M is the bending moment of any cross section on the ring; E is the elastic modulus of the material; I is the inertia moment of the ring cross-sectional plane.

Thus, the bending potential energy is obtained

$$U = \frac{EI}{2r^4} \int_0^{2\pi} \left(\frac{\partial^2 u}{\partial \theta^2} + u\right)^2 r \mathrm{d}\theta \tag{7}$$

In the Equation (7): U is the bending potential energy.

Substitute Equation (3) into Equation (7) and apply the following Equation (8)

$$\begin{aligned} &\int_0^{2\pi} \cos m\theta \cos n\theta \mathrm{d}\theta = 0 \\ &\int_0^{2\pi} \sin m\theta \sin n\theta \mathrm{d}\theta = 0 \ (m \neq n) \\ &\int_0^{2\pi} \cos m\theta \sin m\theta \mathrm{d}\theta = 0 \\ &\int_0^{2\pi} \cos^2 m\theta \mathrm{d}\theta = \int_0^{2\pi} \sin^2 m\theta \mathrm{d}\theta = \pi \end{aligned} \tag{8}$$

Obtain

$$U = \frac{EI\pi}{2r^3} \sum_{\mathrm{i}=1}^{\infty} \left(1 - i^2\right)^2 \left(a_{\mathrm{i}}^2 + b_{\mathrm{i}}^2\right) \tag{9}$$

The kinetic energy of the vibrating ring is

$$T = \frac{A\rho}{2} \int_0^{2\pi} (\dot{u}^2 + \dot{v}^2) r \mathrm{d}\theta \tag{10}$$

In the Equation (10): T is the kinetic energy of the vibrating ring, A is the cross-sectional area of the ring, ρ is the density of the material.

Substitute Equation (3) and (5) into Equation (10) to derive

$$T = \frac{Ar\pi\rho}{2} \sum_{\mathrm{i}=1}^{\infty} (1 + \frac{1}{i^2})(\dot{a}_{\mathrm{i}}^2 + \dot{b}_{\mathrm{i}}^2) \tag{11}$$

Applying Lagrange equation to conservative system and generalized coordinate a_{i}, the differential equation of motion is obtained

$$Ar\pi\rho(1 + \frac{1}{i^2})\ddot{a}_{\mathrm{i}} + \frac{EI\pi}{r^3}(1 - i^2)^2 a_{\mathrm{i}} = 0 \tag{12}$$

Or

$$\ddot{a}_{\mathrm{i}} + \frac{EIi^2(1 - i^2)^2}{\rho A r^4 (1 \div i^2)} a_{\mathrm{i}} = 0 \tag{13}$$

The equation of the same form is obtained for the generalized coordinate b_{i}.

Therefore, the frequency expression for the i-th mode of bending vibration in torus is

$$f_{\mathrm{i}} = \frac{1}{2\pi} \sqrt{\frac{EIi^2(1 - i^2)^2}{\rho A r^4 (1 + i^2)}} \tag{14}$$

The bending vibration mode belongs to the i-th order and recorded as B_{i}. When $i = 1, f_1 = 0$, the ring moves as a rigid body, when $i \geq 2$, the ring vibrate according to the basic bending mode.

The straight and curved beams are composed of two straight beam segments and two semicircular arc segments. As shown in Figure 4, b is the beam width and h is the thickness.

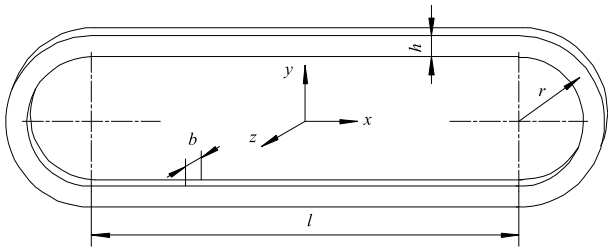

FIGURE 4. Structural diagram of long ring beam.

It is assumed that the beam is uniform and equal section, and the cross-sectional dimension of the beam is very small compared with the centerline radius r. When the antinode number of long ring beam bending vibration mode is 2n, the vibration mode of the bending mode is defined as the n-th order, which is recorded as $\mathrm{B_n}$.

According to the equation $r = (2\pi R_0\text{-}2l)/2\pi$, keep the length of the ring axis as a fixed value, where R_0 is the radius of the ring centerline, set $R_0 = 80$mm, the thickness of the long ring beam $h = 4$ mm, the width $b = 6$ mm, $l/r = 10$, where l is the length of the straight beam section, r is the radius of the ring centerline, the material is brass, the elastic modulus $E = 110\mathrm{GN/m^2}$, the density $\rho = 8400\mathrm{kg/m^3}$, and the unit type is BEAM3. Using the finite element software, the in-plane bending vibration modes of the ring and long ring beam are analyzed, and the $\mathrm{B_2} \sim \mathrm{B_{10}}$ vibration modes and natural frequencies are obtained, the analysis results of ring bending vibration mode are compared with that of long ring beam, as shown in Figure 5.

B. SYMMETRY ANALYSIS OF MODE SHAPES FOR LONG RING BEAMS

Any size combination of long ring structure is selected, When $h = 5$mm, $b = 6$mm, $l = 155$mm, $r = 30$mm, the material is brass, the element type is BEAM3, considering the accuracy requirements, the element scale is 1mm, and the even and odd orders are optional.

Taking $\mathrm{B_{12}}$ and $\mathrm{B_{13}}$ as examples, the coordinate of any node and its displacement in x and y directions are extracted by finite element method to judge the symmetry.

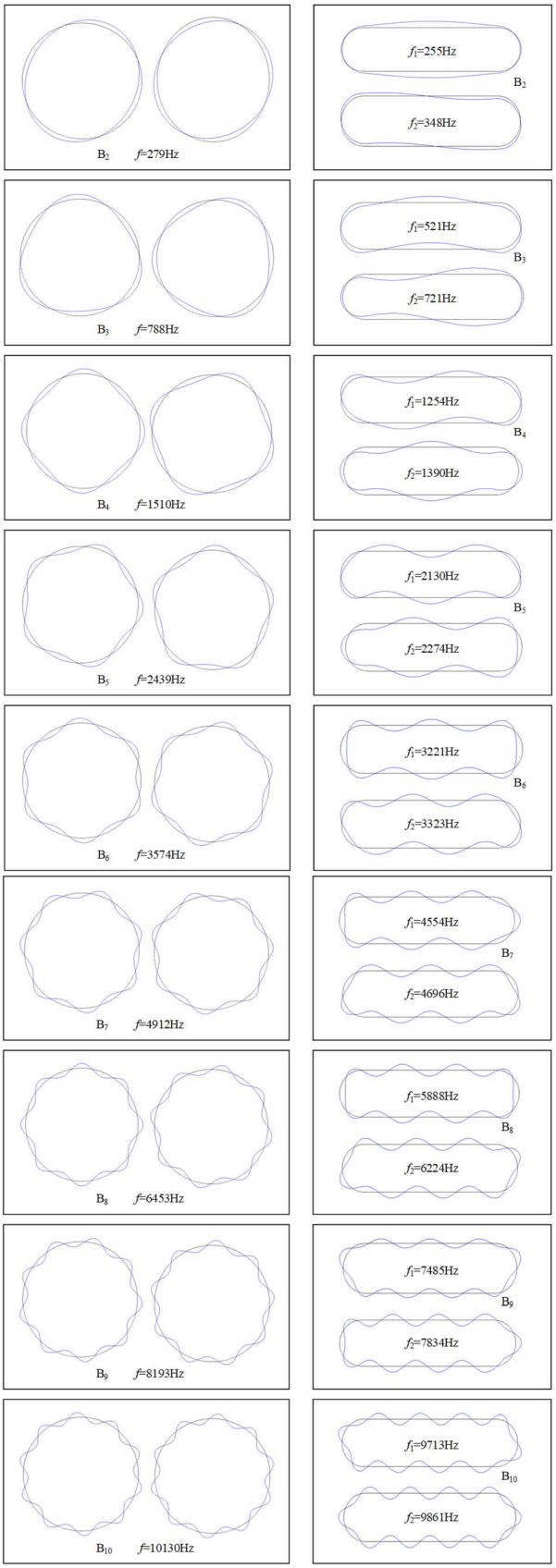

FIGURE 5. In plane bending vibration modes of ring and long ring beam.

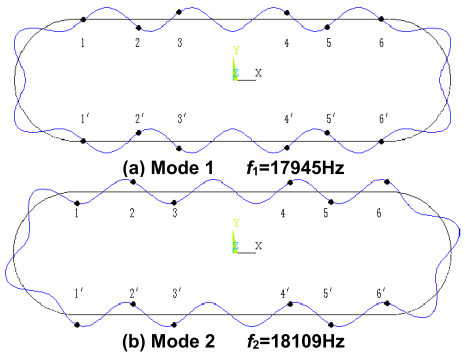

FIGURE 6. In-plane bending vibration modes for B_{12}.

The modal analysis results of B_{12} in-plane bending vibration are shown in Figure 6; the natural frequencies of the two modes are 17945Hz and 18109Hz respectively, with a frequency difference of 164Hz.

Take three nodes 1, 2 and 3 from the upper straight beam section locate in the left half plane, and correspondingly take three nodes 4, 5 and 6 symmetrically on the right half plane, So there are six independent nodes in the upper half plane, and the six nodes 1', 2', 3', 4', 5'and 6' in the lower half plane symmetrical to the upper half plane are also generated in turn.

Table 1 lists the coordinates of the selected node and the deformation of the selected node under two modes.

TABLE 1. Coordinate and deflection of selected nodes for B_{12}.

Point number	Coordinate (mm)	Mode 1		Mode 2	
		△x	△y	△x	△y
1	(-63.5,30)	0.917881 252514	3.78628 5024491	-0.32908 8188785	0.32908 8188802
2	(-42.5,30)	0.969555 795376	-3.75525 3830337	0.18518 6855288	-0.18518 6855275
3	(-6.5,30)	0.201098 867802	-2.13763 3844367	0.78027 4282031	-0.78027 4282034
4	(6.5,30)	-0.20109 8867908	-2.13763 3844530	0.78027 4282025	-0.78027 4282034
5	(42.5,30)	-0.96955 5795399	-3.75525 3830341	0.18518 6855256	-0.18518 6855272
6	(63.5,30)	-0.91788 1252469	3.78628 5024513	-0.32908 8188814	0.32908 8188806
1′	(-63.5,-30)	0.917881 252503	-3.78628 5024485	-0.20343 9525650	-0.20343 9525664
2′	(-42.5,-30)	0.969555 795376	3.75525 3830326	0.23141 3534663	0.23141 3534677
3′	(-6.5,-30)	0.201098 867822	2.13763 3844351	3.12332 2024324	3.12332 2024332
4′	(6.5,-30)	-0.20109 8867888	2.13763 3844537	-3.12332 2024411	-3.123322 024402
5′	(42.5,-30)	-0.96955 5795396	3.75525 3830334	-0.23141 3534864	-0.231413 534848
6′	(63.5,-30)	-0.91788 1252477	-3.78628 5024507	0.20343 9525888	0.203439 525871

Note: △x and △y are the deformation along the x and y directions respectively, as shown in Table 1, and they are relative values.

The observation reveals that the vibration mode of mode 1 is symmetrical about both x-axis and y-axis, and the vibration mode of mode 2 is symmetrical about the origin. The results are consistent with the judgment of theoretical analysis.

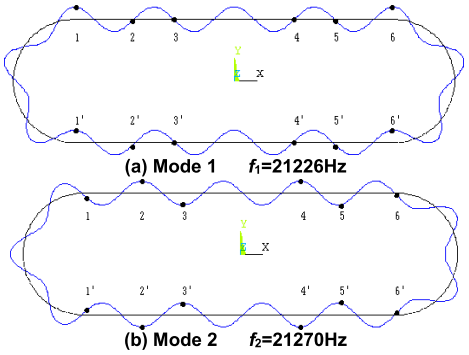

FIGURE 7. In-plane bending vibration modes for B_{13}.

TABLE 2. Coordinate and deflection of selected nodes for B_{13}.

Point number	Coordinate (mm)	Mode 1		Mode 2	
		△x	△y	△x	△y
1	(-72.5,30)	-0.11412 4960147	2.63249 9710575	-0.67040 6996889	-2.79006 3963761
2	(-52.5,30)	-0.23560 9441213	-2.34174 6653457	-0.26972 2903340	3.03687 7812218
3	(-14.5,30)	-0.12840 9589246	-2.72271 4826633	0.64480 0802555	2.72641 6146665
4	(14.5,30)	0.12840 9589129	-2.72271 4825978	0.64480 0802405	-2.72641 6147301
5	(52.5,30)	0.23560 9441262	-2.34174 6652731	-0.26972 2903611	-3.03687 7812753
6	(72.5,30)	0.11412 4960267	2.63249 9709963	-0.67040 6997014	2.79006 3964481
1′	(-72.5,-30)	0.11412 4960275	2.63249 9709970	-0.67040 6996862	2.79006 3964335
2′	(-52.5,-30)	0.23560 9441255	-2.34174 6652801	-0.26972 2903294	-3.03687 7812724
3′	(-14.5,-30)	0.12840 9589110	-2.72271 4826046	0.64480 0802578	-2.72641 6147246
4′	(14.5,-30)	-0.12840 9589255	-2.72271 4826565	0.64480 0802379	2.72641 6146714
5′	(52.5,-30)	-0.23560 9441197	-2.34174 6653382	-0.26972 2903656	3.03687 7812246
6′	(72.5,-30)	-0.11412 4960130	2.63249 9710563	-0.67040 6997039	-2.790063 963910

Note: △x and △y are the deformation along the x and y directions respectively, as shown in Table 2, and they are relative values.

The modal analysis results of B_{13} in-plane bending vibration are shown in Figure 7. The natural frequencies of the two modes are 21226Hz and 21270Hz respectively, and the frequency difference is 44Hz.

The node selection method is the same as B_{12}. Coordinates of selected nodes and deformation of selected nodes in two modes are shown in Table 2.

The observation also reveals that the vibration mode of mode 1 is symmetrical about y-axis, and the vibration mode of mode 2 is symmetrical about x-axis. The results are consistent with the judgment of theoretical analysis.

Through the above symmetry analysis, the order and node selection are arbitrary. Two same order in-plane bending modes at any order are deduced, no matter how different their frequencies are, the conclusion of vibrator symmetry is demonstrated accurately by mathematical method.

C. IN PLANE VIBRATION LAW OF LONG RING BEAM

Starting from the ring with $R_0 = 80$mm, the equation $r = (2\pi R_0\text{-}2l)/2\pi$ is used, the thickness of the long ring beam $h = 4$mm, the width $b = 6$mm, the material is brass, the elastic modulus $E = 110\text{GN/m}^2$, the density $\rho = 8400\text{kg/m}^3$, and the unit type is BEAM3. when l is proportional to r, the variation law of two same order modal natural frequencies for long ring beam is analyzed.

The ratio n of l to r is taken in the range of $0.2\sim 10$ and the step is 0.2. The specific values of n, r and l are listed in Table 3. The vibration modes and natural frequencies of modes B_{15}, B_{16}, B_{17} and B_{18} are analyzed respectively, and the results are shown in Figure 8.

The natural frequencies of two same order vibration modes are generally different, moreover, when the l/r is kept within a certain numerical range, the vibration mode with almost zero frequency difference is found by optimizing the geometric size of the beam. However, when the l/r continued to increase, it is difficult to find the two bending mode with similar frequency.

Keep n constant and double the values of l and r in Table 3 at the same time, the thickness of the long ring beam h is also doubled, and the width b remains unchanged, Starting from the ring with $R_0 = 160$mm, the vibration modes and natural frequencies of modes B_{15}, B_{16}, B_{17} and B_{18} are still analyzed. The results are shown in Figure 9.

It is obvious that the curve in Figure 9 is basically consistent with the corresponding curve in Figure 8, only under the same n value; the two natural frequencies of the same order vibration mode are almost reduced to half of the original size. Therefore, it is inferred that the long ring beam structure maintains both geometric similarity and dynamic similarity.

III. MODAL CONTROL OF SYMMETRICAL CONVEYING VIBRATOR

The key of traveling wave ultrasonic vibration feeding device is to generate unidirectional traveling wave in the vibrator, the condition for synthesizing in-plane bending traveling waves is that two-phase approximately orthogonal in-plane bending vibration modes at the same order of the vibrator are excited, and the natural frequency difference of the two standing waves should be as small as possible. In this paper, parametric modeling is carried out for the prototype of the proposed conveying vibrator by using the finite element software, and the size parameters of some structures are strictly controlled.

A. STRUCTURAL SLOTTING AND VIBRATOR MODE CONTROL

Modal analysis is to find two ideal in-plane bending vibration modes of symmetrical conveying vibrator, and then determine the structural dimensions of each part in the vibrator. Therefore, it is necessary to set the structural parameters before analysis. The specific settings of some parameters during

TABLE 3. Numerical value Of N, R, L.

n	r	l
0.2000	75.2119	15.0424
0.4000	70.9645	28.3858
0.6000	67.1712	40.3027
0.8000	63.7629	51.0103
1.0000	60.6838	60.6838
1.2000	57.8883	69.4660
1.4000	55.3390	77.4747
1.6000	53.0049	84.8078
1.8000	50.8596	91.5473
2.0000	48.8812	97.7625
2.2000	47.0510	103.5123
2.4000	45.3529	108.8470
2.6000	43.7731	113.8101
2.8000	42.2997	118.4391
3.0000	40.9222	122.7666
3.2000	39.6316	126.8211
3.4000	38.4199	130.6277
3.6000	37.2801	134.2084
3.8000	36.2060	137.5829
4.0000	35.1921	140.7683
4.2000	34.2334	143.7801
4.4000	33.3255	146.6322
4.6000	32.4646	149.3370
4.8000	31.6470	151.9055
5.0000	30.8696	154.3478
5.2000	30.1294	156.6730
5.4000	29.4240	158.8893
5.6000	28.7508	161.0042
5.8000	28.1077	163.0245
6.0000	27.4927	164.9564
6.2000	26.9041	166.8056
6.4000	26.3402	168.5772
6.6000	25.7994	170.2762
6.8000	25.2804	171.9067
7.0000	24.7818	173.4729
7.2000	24.3026	174.9786
7.4000	23.8415	176.4271
7.6000	23.3976	177.8217
7.8000	22.9699	179.1653
8.0000	22.5576	180.4607
8.2000	22.1598	181.7104
8.4000	21.7758	182.9167
8.6000	21.4049	184.0820
8.8000	21.0464	185.2082
9.0000	20.6997	186.2974
9.2000	20.3643	187.3512
9.4000	20.0395	188.3714
9.6000	19.7250	189.3596
9.8000	19.4201	190.3173
10.0000	19.1246	191.2458

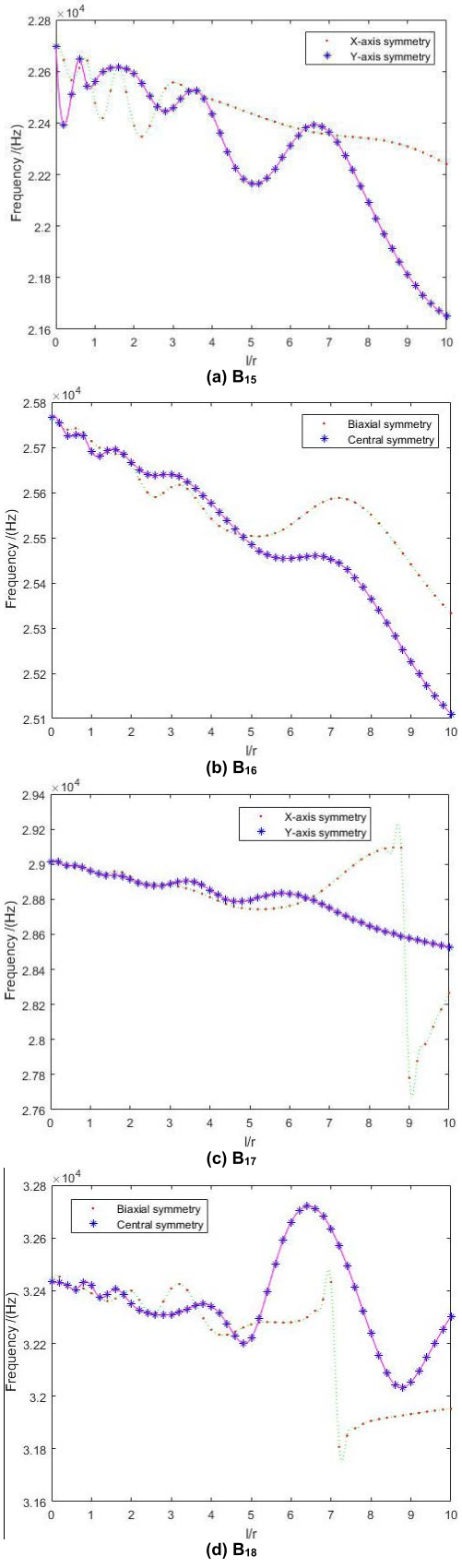

FIGURE 8. Change of natural frequencies for the same two order modes with l and r.

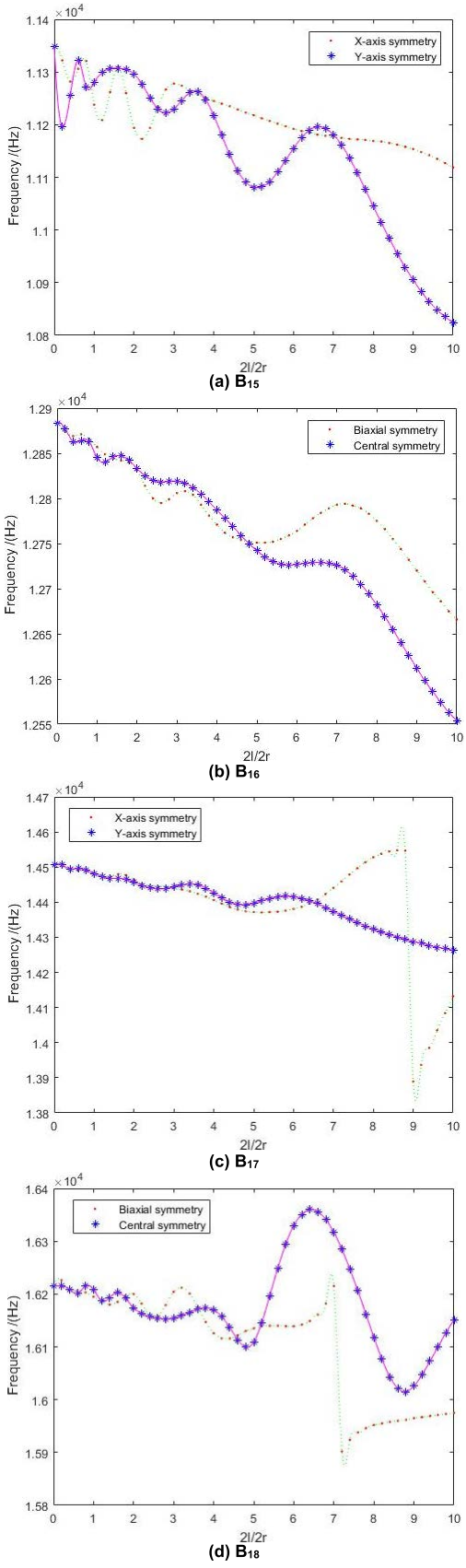

FIGURE 9. Change of natural frequencies for the same two order modes with 2l and 2r.

finite element analysis are shown in Table 4. In finite element analysis (without considering the influence of bonding layer), SOLID45 eight node hexahedron element is adopted for elastomer, SOLID5 electromechanical coupling element is adopted for piezoelectric ceramics, mapping mode is adopted for meshing, and the element size is specified as 1mm.

TABLE 4. Setting of partial parameter in finite element analysis.

Parts	Elastic modulus GPA	Density(kg/m^3)	Poisson's ratio
Elastomer (brass 59)	1.1	8400	0.3
Piezoelectric ceramics (pzt-181)	anisotropy	7850	

The partial enlarged view of the tooth part in the symmetrical conveying vibrator is shown in Figure 10. In the Figure 10, l_1 is the tooth length of the vibrating elastomer, l_2 is the tooth gap, h_1 is the substrate thickness, h_2 is the tooth height, and c is the tooth gap spacing. Since the condition for synthesizing in-plane bending traveling waves is to find two bending vibration standing waves with equal frequency and amplitude and 90° difference between space and time [21], [22], the length sum of the tooth and the tooth gap is strictly controlled to meet the quarter wavelength in the parametric design [23], and there is $c = l_1 + l_2 = \lambda/4$ in the corresponding figure. At the same time, the perimeter of the vibrator is an integral multiple of the bending vibration wavelength, so as to reduce the difficulty of searching [24].

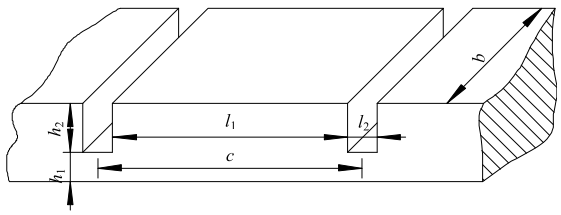

FIGURE 10. Partial enlarged drawing of vibrator tooth.

It is found that no matter how to adjust and combine the size parameters; it is difficult to find two ideal bending vibration modes. When the frequency difference decreases, the corresponding vibration mode is not ideal, but when the vibration mode is more reasonable, the frequency difference is very different, and some vibration modes also have obvious wavelength non-uniformity, and even other order vibration modes are mixed between the two same order modes.

At the same time, it is required that the symmetrical conveying vibrator is modular combined in the width direction [25], so it is necessary to take into account the transverse vibration of the vibrator in the width direction. In fact, there is obvious bending vibration in the width direction. The key factor causing the bending vibration mode of the vibrator is the structure of the ceramic sheet and its bonding

position [26]. Therefore, the whole ceramic sheet is replaced with independent small ceramic sheets. However, it is found that the position accuracy of ceramic sheet paste to vibrator is difficult to ensure [27].

Therefore, it is envisaged that proper slotting on the matrix surface of the vibrator elastomer can improve the positioning accuracy of the ceramic sheet on the one hand[28] [29], it is expected that the modal correction is achieved while shortening the analysis process on the other hand [30], such as the structural diagram of slotted vibrator with independent piezoceramics is shown in Figure 11.

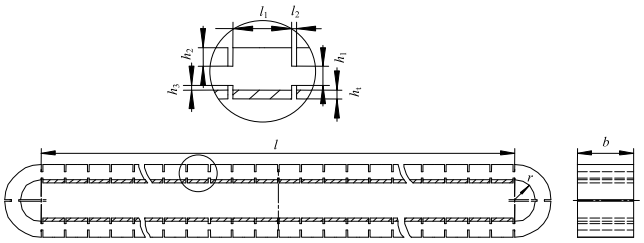

FIGURE 11. Structure diagram of slotted vibrator with independent piezoceramics.

Through the strict control of size parameters, the B_{18} bending mode of the vibrator is finally optimized. The vibrator width b is 16mm, the length of the upper and lower straight beam sections l is 208.5mm, the matrix thickness h_1 and tooth height h_2 are 2mm, the tooth length l_1 and the ceramic sheet length are 6mm, the tooth gap l_2 is 0.5mm, the groove depth h_3 and groove length are 0.5mm, the ceramic sheet thickness h_t is 1mm, and the number of teeth contained in the upper and lower straight beam sections is 32.

Because the large frequency difference is not conducive to the synthesis of traveling waves, it is necessary to adjust some geometric dimensions of the vibrator to reduce the frequency difference without affecting the vibration mode.

Through parameter analysis, it is found that the inner radius of the circular arc at both ends r is the best optimization object. Therefore, the inner radius of the circular arc at both ends r is adjusted slightly, and finally set to 5.3mm; the final result of finite element analysis is shown in Figure 12.

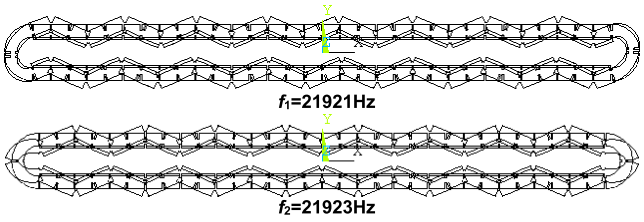

FIGURE 12. Orthogonal modes of conveying vibrator for B_{18}.

The shape of the vibrator before and after deformation is shown in Figure 12. The natural frequencies of the two orthogonal modes are 21921Hz and 21923Hz respectively, and the frequency difference is 2Hz.

It is observed that the tooth gap at the antinode and the slotting are basically maintained in the same vertical direction before and after deformation. Therefore, the slotting treatment of the vibrator elastomer can effectively control the bending vibration mode of the vibrator.

B. OPTIMAL DESIGN OF SYMMETRICAL CONVEYING VIBRATOR

A vibrator structure with 32 teeth in both the upper and lower straight beam sections is determined by the finite element analysis. However, by observing the B_{18} vibration mode of the vibrator, it is found that the waveform of each standing wave is very similar to that of the Saw tooth wave, but in fact, the two standing wave waveforms constituting traveling wave are similar to sinusoidal waveforms.

During the analysis, the reason for this phenomenon is that the length ratio between the tooth and its gap is too large. In addition, increasing the number of teeth on the vibrator surface is conducive to increase the transverse amplitude of the vibrator.

Therefore, the teeth number of this structure vibrator is adjusted, that is, a tooth gap is added at the center of the original tooth, and the corresponding number of teeth is doubled. The structure diagram of the modified vibrator is shown in Figure 13.

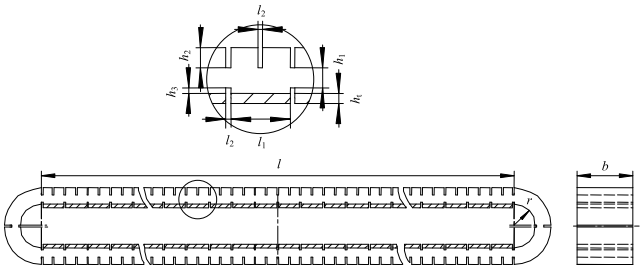

FIGURE 13. Structure diagram of modified vibrator after slotting.

The vibration modes of the two vibrator modes are shown in Figure14. By observing the finite element analysis results, it is found that the increases of tooth gap effectively reduce the bending stiffness of the vibrator, but it doesn't affect the vibration order of the conveying vibrator, which is still B_{18}. Slightly adjust the inner radiuses of the arc at both ends r to 5.9mm, the natural frequencies are 20326Hz and 20327Hz respectively, the frequency difference is 1Hz. obviously, the vibration mode in Figure 14 is significantly improved compared with Figure 12.

C. SENSITIVITY ANALYSIS OF VIBRATOR GEOMETRY ON VIBRATION MODE

In the production process, when there are strict requirements on the conveying width, the vibrator width is adjusted; however, with the increasing of conveying width, transverse bending vibration occurs in the width direction of vibrator. Therefore, it is required that the conveying vibrator is modular combined in the width direction, the conveying width

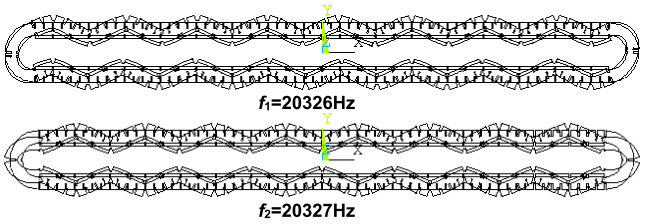

FIGURE 14. Orthogonal modal of modified vibrator for B_{18} afterslotting.

is designed within the size range without large transverse bending vibration.

In order to select the best design width of the vibrator and keep the other dimensions of the vibrator structure in Figure 13 unchanged, only change the dimensions in the width direction. Observe the bending mode of the vibrator from the ANSYS figure. It is found that the corresponding vibration modes under different widths are very similar, but the deformation in the width direction is slightly different.

Therefore, the width dimensions are designed in series, the vibrator natural frequencies and frequency differences of the two bending modes under different widths are shown in Table 5.

TABLE 5. Natural frequency and frequency difference of two modes for vibrator with different width.

Width (mm)	Mode 1 frequency (Hz)	Mode 2 frequency (Hz)	Frequency difference (Hz)
14	20301	20299	2
15	20314	20313	1
16	20327	20326	1
17	20338	20339	1
18	20349	20350	1
19	20359	20360	1
20	20368	20370	2
21	20376	20379	3
22	20384	20388	4

Compare the modes of different models, and finally, the vibrator structure with a width of 16mm is selected as the object of solid processing.

The vibration mode is closely related to the design of the conveying vibrator; the parameter sensitivity of geometric size on the B_{18} mode of vibrator is analyzed. Corresponding to Figure 13, the main objects of analysis are: vibrator substrate thickness is h_1, tooth height is h_2, boss height is h_3, inner radius of arc at both ends is r, tooth gap is l_2 and piezoelectric ceramic thickness is h_t. During the analysis, ensure that other dimensions of the vibrator remain unchanged, change any one size of the analysis object and observe the influence of the size on the mode, and adjust the step size is 0.1mm, The analysis results are shown in Figure 15.

It is found out from Figure 15 that the coincidence degree of every two curves under the substrate thickness h_1, tooth height h_2, tooth gap l_2 and piezoelectric ceramic thickness h_t are better, indicating that the change of these parameters have little effect on natural frequency difference between two modes, which is relaxes when considering the machining accuracy. But from Figure 15 (c) and (d), it is seen that the variation of h_3 and r have a great influence on the natural frequency difference between the two modes, so the dimensional accuracy should be strictly controlled during machining. Through parameter sensitivity analysis, it is found that the inner radius of the circular arc at both ends r is the best optimization object, and finally set to 5.9mm; The above analysis results not only shows the sensitivity of geometric dimensions to vibrator modes, but also provides a theoretical basis for the design of this type conveying vibrator in the future.

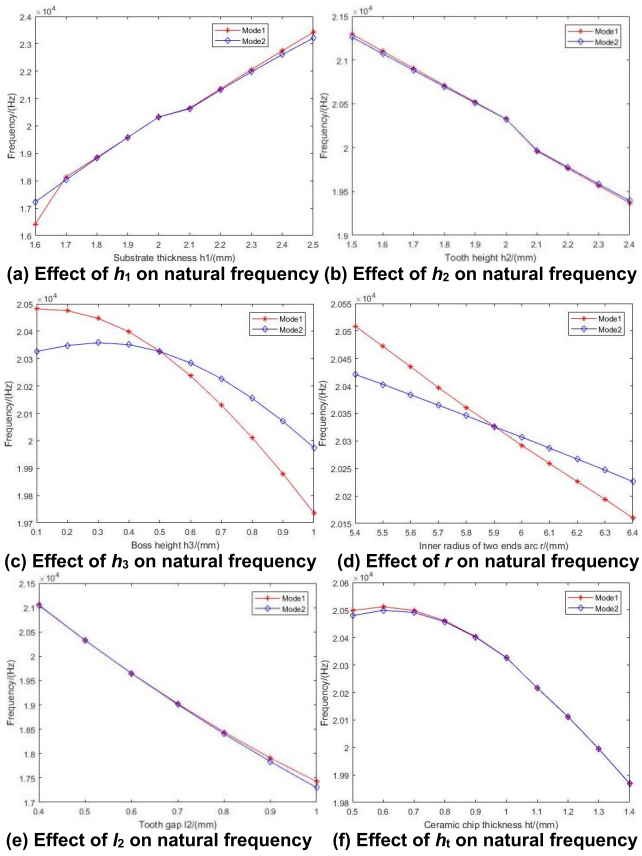

(a) Effect of h_1 on natural frequency (b) Effect of h_2 on natural frequency

(c) Effect of h_3 on natural frequency (d) Effect of r on natural frequency

(e) Effect of l_2 on natural frequency (f) Effect of h_t on natural frequency

FIGURE 15. Parameter sensitivity analysis of vibrator modes.

IV. WHOLE MACHINE EXPERIMENT OF ULTRASONIC VIBRATION FEEDING DEVICE

The ultrasonic vibration feeding device is mainly composed of conveying vibrator, support structure and support. The physical drawing of the prototype is shown in Figure 16, the conveying vibrator is overlapped in the through hole of the support through the support rod, and the support rod and the support are fastened with screws.

The prototype design adopt 64 independent ceramic sheets, and two fixtures with the same structure are designed and manufactured for the pasting of ceramic sheets, as shown

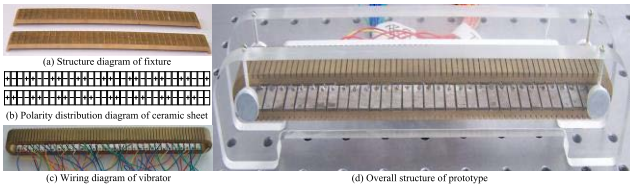

FIGURE 16. Physical drawing of overall prototype.

in Figure 16 (a); The polarity (+ - sign represent the polarization direction of the ceramic sheet) and position are shown in Figure 16 (b), the piezoelectric ceramics are accurately arranged in the groove of the fixture with plastic film and double-sided adhesive tape; the wiring of the prototype is welded, as shown in Figure 16 (c). Each piece of piezoelectric ceramic is welded with a wire, and the ground wire is led out from the substrate.

A. EXPERIMENTAL INSTRUMENTS AND SCHEME

The experimental device and test scheme are shown in Figure 17. The sinusoidal signal is generated by the signal generator, and the appropriate voltage is output by the power amplifier, and load onto the piezoelectric ceramic chip of the conveying vibrator, the vibration information is transmitted to the oscilloscope by the laser vibrometer, and the amplitude of vibration is displayed in the oscilloscope.

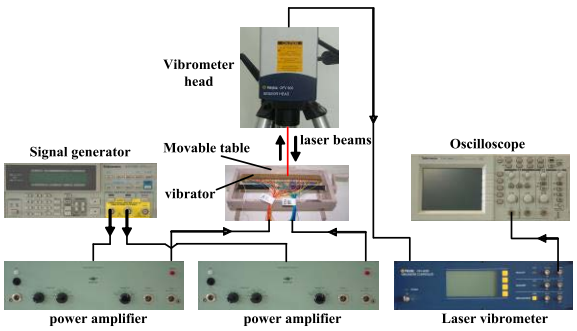

FIGURE 17. Wiring diagram of experimental device.

Before the test, each part of the vibrator is calibrated: the surface where the red and yellow leads are located is regarded as side A and define as the upper straight beam section, and the surface where the blue and green leads are located is regarded as side B and defined as the lower straight beam section accordingly; The ceramic chips weld with the red and yellow leads are marked as group A, and the corresponding ceramic chips weld with the blue and green leads are marked as group B, as shown in Figure 18.

B. RESONANCE FREQUENCY TEST OF PROTOTYPE

Through finite element analysis and calculation, the resonant frequencies of the B_{18} order two modes are 20326Hz and 20327Hz respectively. One group of ceramic sheets is excited, a fixed point is selected on a conveying surface of the vibrator, the frequency of the signal generator is adjusted near the

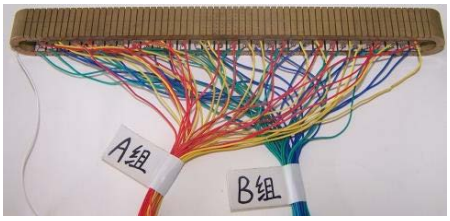

FIGURE 18. Schematic diagram of vibrator lead grouping.

resonant frequency of the theoretical analysis, and several resonance frequency points are found. It is tested that the B_{18} order two-phase working frequencies of the vibrator are 18330Hz and 18420Hz respectively, and the frequency difference is 90Hz. There is a certain deviation compared with the frequency value of theoretical analysis. There are many possible reasons for this phenomenon, such as the adhesive layer is not considered in the finite element modeling, the selection of grid size in finite element analysis, the setting of material parameters, and subsequent processing errors, the position error when the piezoelectric ceramic is pasted with the vibrator elastomer, etc.

C. TESTING OF MODAL CONTROL

In order to quantitatively verify whether the actual working mode of the conveying vibrator was consistent with the theoretical analysis; That was, whether the real modal control was achieved, it was necessary to analyze the amplitude distribution of the vibrator tooth surface and the orthogonality of the vibrator's two-phase modes.

1) ORTHOGONALITY OF TWO-PHASE MODES

In order to verify the existence of orthogonality in the theoretical analysis, the data in the length direction amplitude test are extracted, as shown in Figure 19 (a) and (b). It is found that the actual working mode has good orthogonality.

2) AMPLITUDE DISTRIBUTION ALONG THE LENGTH

Set the input voltage peak value as 40V, excite the ceramic sheets of groups A and B respectively, and the excitation frequencies are 18350Hz and 18440Hz respectively. On the symmetrical plane of the vibrator, on the symmetrical plane of the vibrator, starting from the position of the first tooth at the left end of the working face, took three points on each tooth as the test point, a total of 64 teeth, i.e. 192 test points. Record the voltage peak value of each test point, and then convert it into amplitude. According to this method, the amplitude distribution of the tooth surface along the length of A and B side is tested respectively, as shown in Figure 20 and Figure 21.

In the figures, the thick line represents the actually measured amplitude curve, and the dotted line represents the amplitude curve of finite element analysis. Since the actually measure amplitude values are positive, it isn't convenient to compare with the finite element analysis results, the actual

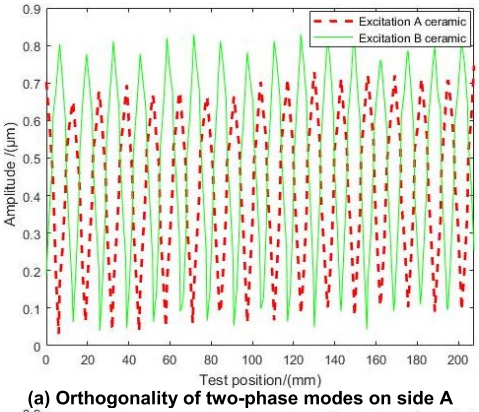

(a) Orthogonality of two-phase modes on side A

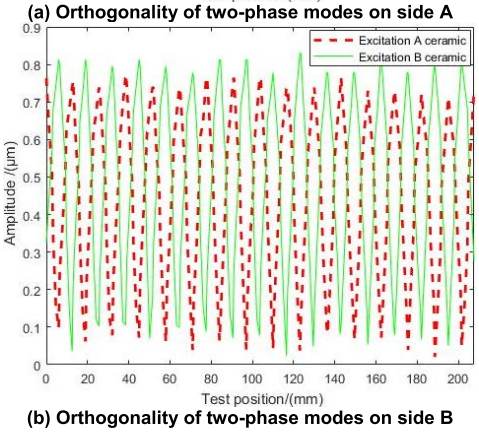

(b) Orthogonality of two-phase modes on side B

FIGURE 19. Orthogonality of two-phase modes.

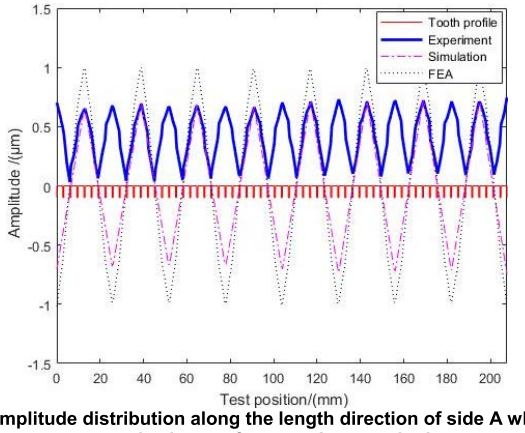

(a) Amplitude distribution along the length direction of side A when ceramic sheets of groups A are excited

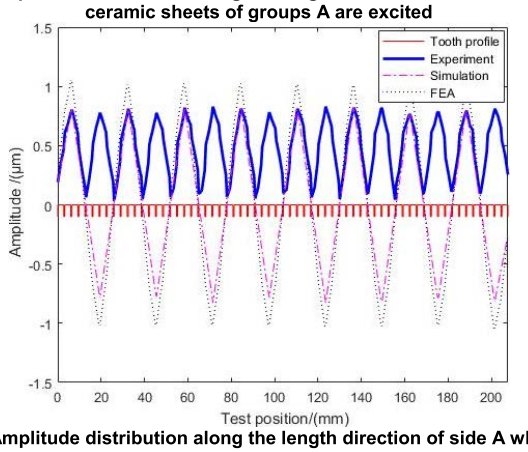

(b) Amplitude distribution along the length direction of side A when ceramic sheets of groups B are excited

FIGURE 20. Amplitude distribution along the length direction of side A.

measure amplitude curve is simulated and represented by dotted lines, and the thin line represents the tooth profile curve.

As illustrated in Figure 20 and Figure 21, the actual working mode is basically the same as that of the finite element analysis, and the side A and B achieve good modal control.

3) AMPLITUDE DISTRIBUTION IN WIDTH DIRECTION

In theoretical analysis, Not only observe the vibration mode in the length direction, but also pay attention to the vibration mode in the width direction. Set the input voltage peak value as 40V, excite the ceramic sheets of groups A and B respectively, and the excitation frequencies are 18340Hz and 18420Hz respectively, Select a wavelength range (take the middle part of the vibrator structure) on the working face, a total of 8 teeth, select the center position of each tooth along the width direction, and select 7 points at each center position (take from the side close to the lead), a total of 56 test points, record the voltage peaks of each test point, and then convert them into amplitude. Test the amplitude distribution along the width direction of side A and B according to this method, as shown in Figure 22 and Figure 23.

The amplitude distribution along the length direction of the tooth widths is shown in Figure 22 (a) and (c). However, the curves shown in Figure 22 (a) are not uniform, the amplitude drop of each tooth along the tooth width direction is large, and the curves in Figure 22 (c) are relatively better. IN order to more intuitively describe the amplitude distribution in the width direction, the amplitude distribution of each tooth along the center of the tooth width is shown in Figure 22 (b) and (d). Only the amplitude curve of individual teeth along the width direction has no obvious warping In Figure 22 (b), while the curve is relatively stable in Figure 22 (d).

Although there are similar problems in Figure 23, it is better than in Figure 22. Since the test is carried out only within one wavelength range of the vibrator working face, and there are individual warps in the width direction, there is no large bending deformation in the width direction for the whole conveying vibrator.

D. PERFORMANCE TEST AND ANALYSIS OF PROTOTYPE

The conveying performance of the whole device depends on the conveying rate, and it is an important standard to judge whether the conveying vibrator structure is feasible and achieve optimization.

1) FREQUENCY-AMPLITUDE CHARACTERISTICS

In order to analyze the Frequency-amplitude characteristics of the conveyor, Select a fixed point on side A of the vibrator and set the peak value of the two-phase input voltage at 40V, the ceramic sheets of group A are excited, the working

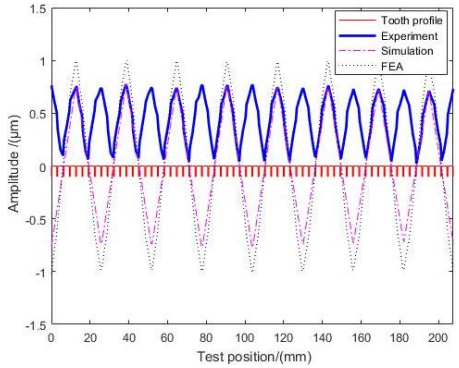

(a) Amplitude distribution along the length direction of side B when ceramic sheets of groups A are excited

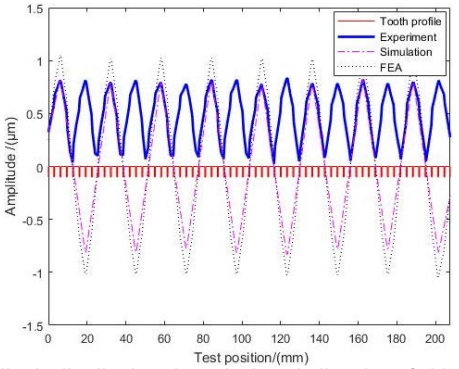

(b) Amplitude distribution along the length direction of side B when ceramic sheets of groups B are excited

FIGURE 21. Amplitude distribution along the length direction of side B.

frequency of phase A is 18350Hz as the reference value, adjust the frequency of the signal generator in steps of 100Hz, and record the corresponding amplitude value at each frequency. Similarly, the ceramic sheets of group B are excited, record the corresponding amplitude value at each frequency, draw the Frequency-amplitude characteristic curve, and fit the curve. The results are shown in Figure 24.

As shown in Figure 24, with the increase of working frequency, the amplitude of the conveying vibrator tooth surface also increases; when the working frequency reaches the resonant frequency of the system, the amplitude of the conveying vibrator tooth surface reaches the maximum; when the working frequency continues to increase, the amplitude of the conveying vibrator tooth surface is shown a decreasing trend.

2) RELATIONSHIP BETWEEN AMPLITUDE AND CONVEYING RATE

The conveying rate is an important standard to measure the conveying capacity of ultrasonic vibration feeding device, and the conveying rate is closely related to the amplitude of the conveying vibrator surface.

Select side A of the conveying vibrator for test. The conveying material is tapered roller, and the excitation frequency of the vibrator is set as the average value of two-phase

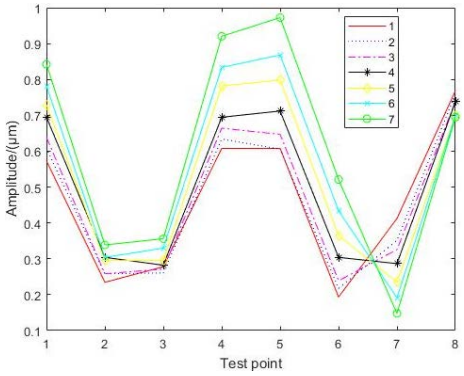

(a) Amplitude distribution along the length direction of different positions of tooth width on side A when ceramic sheets of group A are excited

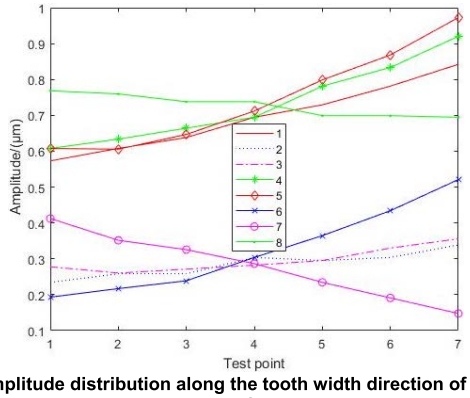

(b) Amplitude distribution along the tooth width direction of side A when ceramic sheets of group A are excited

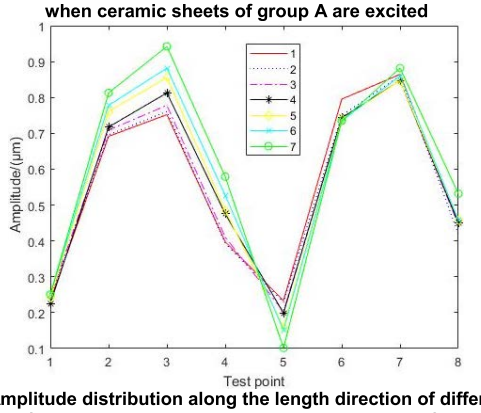

(c) Amplitude distribution along the length direction of different positions of tooth width on side A when ceramic sheets of group B are excited

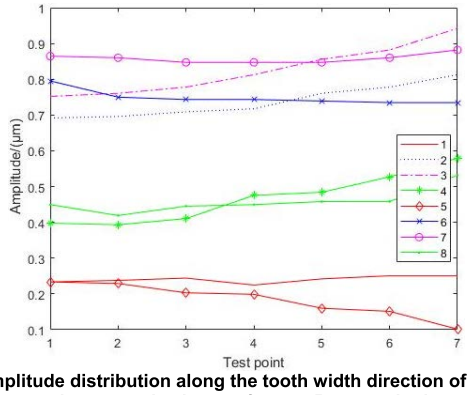

(d) Amplitude distribution along the tooth width direction of side A when ceramic sheets of group B are excited

FIGURE 22. Amplitude distribution along the width direction of side A.

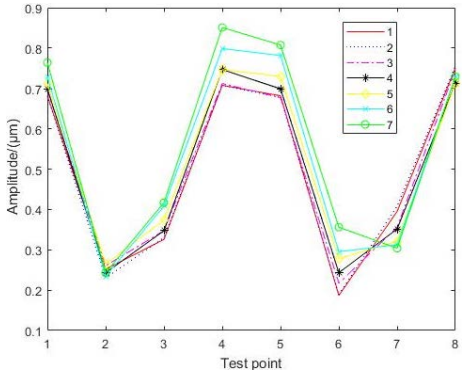

(a) Amplitude distribution along the length direction of different positions of tooth width on side B when ceramic sheets of group A are excited

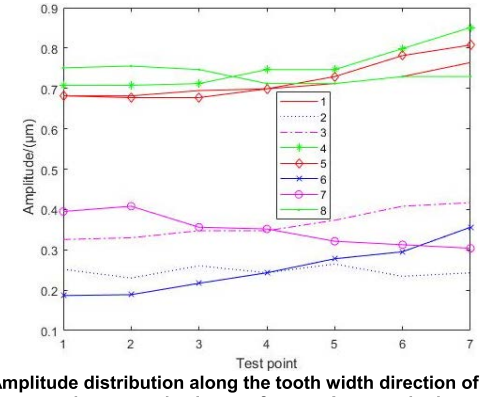

(b) Amplitude distribution along the tooth width direction of side B when ceramic sheets of group A are excited

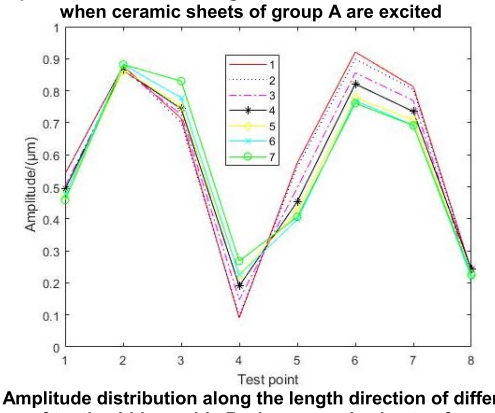

(c) Amplitude distribution along the length direction of different positions of tooth width on side B when ceramic sheets of group B are excited

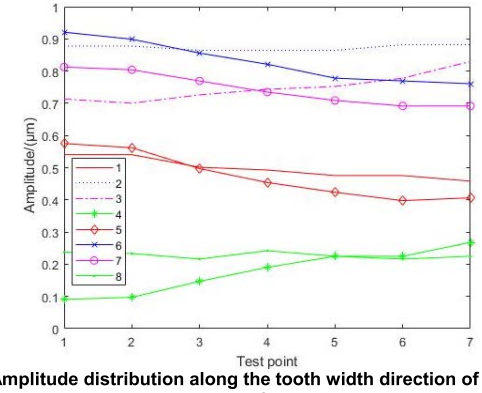

(d) Amplitude distribution along the tooth width direction of side B when ceramic sheets of group B are excited

FIGURE 23. Amplitude distribution along the width direction of side B.

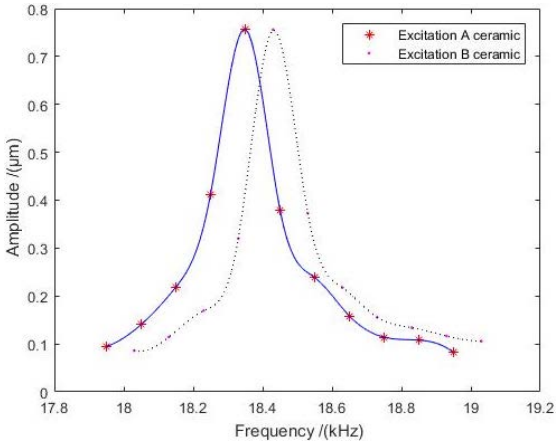

FIGURE 24. Frequency-amplitude characteristic.

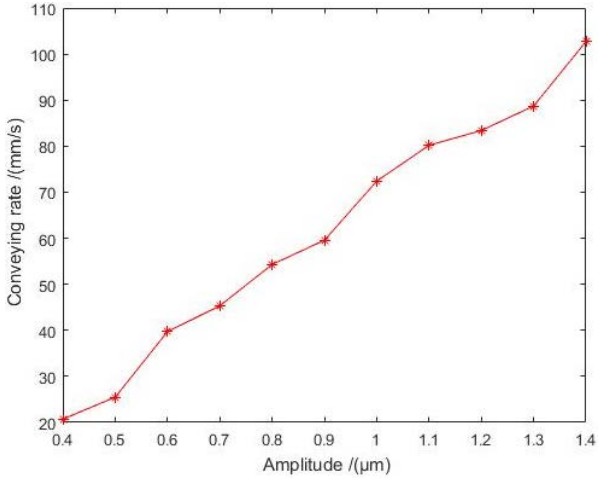

FIGURE 25. Relationship between amplitude and conveying rate.

working frequency is 18390Hz, Starting from an amplitude of 0.4μm, with Step size 0.1μm to calibrate the amplitude, The corresponding voltage peaks under different amplitudes are obtained, and the conveying vibrator is moved to find the peak positions of two standing waves when the two-phase of the vibrator are excited respectively; By adjusting the power amplifier, the voltage peak of the particle at the standing wave peak position is consistent with the voltage peak corresponding to the calibrated amplitude, and measure the conveying rate under different amplitudes, the relationship curve between amplitude and conveying rate is obtained, as shown in Figure 25. The conveying rate of ultrasonic vibration feeding device increases with the amplitude increasing of vibrator surface.

3) EFFECT OF MATERIALS ON CONVEYING RATE

Using the above test method of conveying rate, the excitation frequency is set at 18390Hz, and the amplitude of the particle on the vibrator surface is adjusted to 1μm, the conveying

TABLE 6. Transportability Of different materials.

Material type	Material characteristics	Conveying rate (mm/s)
Cap nut (M8)	The material was stainless steel, the surface was very smooth, the quality was heavier, and it was easy to transport	79.28
Hexagon nut (M5)	The material was steel, with smooth surface, light weight and easy transportation	67.48
Bearing (604)	The material was stainless steel with smooth surface and easy transportation	74.20
Tapered roller (2.6g)	The material was stainless steel, the surface was smooth and easy to transport	77.51
Shim (0.2g)	The material was stainless steel, the surface was very smooth and easy to transport	75.82
Huangyao tablet (Ø10,0.5g)	The surface was smooth, the shape was large, and it was easy to transport	65.57
Baiyao tablet (Ø7,0.1g)	Rough surface, small shape, difficult to transport	53.32

performance of the ultrasonic vibration feeding device is tested for several materials with different materials such as material, size, mass, density, shape and surface roughness. The results are shown in table 6.

The experimental results show that the ultrasonic vibration feeding device has a certain selectivity to the conveying object, The same prototype has good conveying performance for materials with smooth surface and heavy quality, such as cap nuts (M8) and tapered rollers; For materials with smooth surface and light weight, such as hexagon nut (M5), bearing (604), gasket and other materials, the conveying performance is general; for materials with rough surface and light weight, such as tablets, the conveying performance is poor, and some materials can hardly be transported.

It is seen that the ultrasonic vibration feeding device designed in this paper is suitable for conveying materials with smooth surface and heavy mass.

V. CONCLUSION

In this paper, a new scheme of ultrasonic vibration feeding device with double symmetrical axis structure is proposed, a systematic theoretical analysis is carried out for the conveying vibrator, the principle prototype of ultrasonic vibration feeding device is made, and a large number of experimental studies are carried out. The main conclusions of this paper are summarized as follows:

Taking the finite element software ANSYS as the main tool, the in-plane bending vibration modes of ring and long ring beam are compared and analyzed. The vibration mode symmetry of long ring beam is demonstrated by mathematical method, the inherent law of in-plane bending vibration of long ring beam is explored, and finally the prototype of symmetrical conveying vibrator is proposed.

In the dynamic design process of the conveying vibrator, the principle of quarter wavelength is strictly followed, and a feasible scheme that can control the vibration mode of the vibrator is proposed, that is, the elastomer surface of the vibrator is properly slotted, so as to force the antinode position of the vibration mode to make the conveying vibrator work in the ideal mode. The experimental verification proves the feasibility of the mode control method; it provides a theoretical basis for the design of this type conveying vibrator in the future.

Through the modal analysis of finite element software, Two B_{18} order in-plane bending vibration modes of the vibrator are found, the natural frequencies are 20326Hz and 20327Hz respectively, and the frequency difference is only 1Hz, which meets the engineering requirements. By using the design method of pasting independent ceramic sheets, the transverse vibration in the width direction of the vibrator is minimized, which provides a basis for the serialization design of width dimensions. The influence of the main geometric size of the vibrator on the B_{18} order bending mode is analyzed. The analysis shows that the substrate thickness, tooth height, tooth gap and piezoelectric ceramic thickness of the vibrator has little influence on the natural frequency difference between the two modes, while the boss height of the vibrator and the inner radius of the arc at both ends has a great influence on the natural frequency difference between the two modes.

According to the results of theoretical analysis, the principle prototype is developed, and the resonant frequency and vibration mode of the prototype are experimentally studied. The experimental results show that the B_{18} order two-phase working frequencies of the vibrator are 18330Hz and 18420Hz respectively, and the frequency difference is 90Hz. There is a certain deviation compare with the frequency difference of theoretical analysis, but this deviation is within the allowable range. The amplitude distribution of the conveying vibrator tooth surface is studied. The results show that the actual working mode is basically consistent with the finite element analysis results. From the perspective of traveling wave synthesis, the existence of orthogonality in theoretical analysis is verified.

The conveying performance of ultrasonic vibration feeding device is tested, and the effects of amplitude and material type on the conveying rate are analyzed. The experimental results show that there is an approximate linear relationship between the conveying rate and the amplitude of vibrator surface; under the same working frequency and amplitude, different kinds of materials are selected for the conveying capacity test, and the results show that different conveying

objects has different conveying rates, and the conveying effect is better for materials with smooth surface and heavy quality.

REFERENCES

[1] H. Li, W. Chen, X. Tian, and J. Liu, "An experiment study on temperature characteristics of a linear ultrasonic motor using longitudinal transducers," *Ultrasonics*, vol. 95, pp. 6–12, May 2019.

[2] L.-K. Chang and M.-C. Tsai, "Design of single-phase driven screw-thread-type ultrasonic motor," *Rev. Sci. Instrum.*, vol. 87, no. 5, May 2016, Art. no. 055002.

[3] X. C. Chu, J. Wang, S. Yuan, L. Li, and H. Cui, "A screw-thread-type ultrasonic actuator based on a Langevin piezoelectric vibrator," *Rev. Sci. Instrum.*, vol. 85, no. 6, Jun. 2014, Art. no. 065002.

[4] Y. He, Z. Yao, S. Dai, and B. Zhang, "Hybrid simulation for dynamic responses and performance estimation of linear ultrasonic motors," *Int. J. Mech. Sci.*, vols. 153–154, pp. 219–229, Apr. 2019.

[5] C. Jiang, X. Wu, D. Lu, Z. Xu, and L. Jin, "Contact modeling and performance evaluation of ring type traveling wave ultrasonic motors considering stator teeth," *Ultrasonics*, vol. 117, Dec. 2021, Art. no. 106518.

[6] Y. Deng, G. Zhao, X. Yi, and W. Xiao, "Contact modeling and input-voltage-region based parametric identification for speed control of a standing wave linear ultrasonic motor," *Sens. Actuators A, Phys.*, vol. 295, pp. 456–468, Aug. 2019.

[7] Y. Tanoue and T. Morita, "Opposing preloads type ultrasonic linear motor with quadruped stator," *Sens. Actuators A, Phys.*, vol. 301, Jan. 2020, Art. no. 111764.

[8] J. L. Fan, Y H. Zhang, and Y. H. Zhou, "Study on a novel in-plane longitudinal-bending compound linear ultrasonic motor," *Piezoelectrics Acoustooptics*, vol. 41, no. 6, pp. 819–823, 829, Dec. 2019.

[9] R. Niu, H. Zhu, and C. Zhao, "A four-legged linear ultrasonic motor: Design and experiments," *Rev. Sci. Instrum.*, vol. 91, no. 7, Jul. 2020, Art. no. 076107.

[10] B. Zhang, Z. Yao, Z. Liu, and X. Li, "A novel L-shaped linear ultrasonic motor operating in a single resonance mode," *Rev. Sci. Instrum.*, vol. 89, no. 1, Jan. 2018, Art. no. 015006.

[11] S. Izuhara and T. Mashimo, "Characterization of bulk piezoelectric element-based ultrasonic motors," *ROBOMECH J.*, vol. 7, no. 1, p. 31, Aug. 2020.

[12] S. Miyake, Tomohiro Harada, Hiroyuki Shimizu, Sumiaki Kishimoto, and Takeshi Morita, "High-power characteristics of (Bi, Na) TiO_3-$BaTiO_3$ ceramics and application in miniature ultrasonic motor," *Sensors Mater.*, vol. 32, no. 7, pp. 2443–2452, Jul. 2020.

[13] R. Niu, J. Liu, H. Zhu, and C. Zhao, "Design and evaluation of a novel light arc-shaped ultrasonic motor," *AIP Adv.*, vol. 9, no. 6, Jun. 2019, Art. no. 065009.

[14] F. Wang, U. Nishizawa, H. Tanaka, and S. Toyama, "Development of miniature spherical ultrasonic motor using wire stators," *J. Vibroeng.*, vol. 20, no. 8, pp. 2939–2950, Dec. 2018.

[15] K. Miyoshi and T. Mashimo, "Miniature direct-drive two-link using a micro-flat ultrasonic motor," *Adv. Robot.*, vol. 32, no. 20, pp. 1102–1110, Sep. 2018.

[16] Y. Liu, S. Shi, C. Li, W. Chen, and J. Liu, "A novel standing wave linear piezoelectric actuator using the longitudinal-bending coupling mode," *Sens. Actuators A, Phys.*, vol. 251, pp. 119–125, Nov. 2016.

[17] M. Kucera, E. Wistrela, G. Pfusterschmied, V. Ruiz-Díez, T. Manzaneque, J. Hernando-García, J. L. Sánchez-Rojas, A. Jachimowicz, J. Schalko, A. Bittner, and U. Schmid, "Design-dependent performance of self-actuated and self-sensing piezoelectric-AlN cantilevers in liquid media oscillating in the fundamental in-plane bending mode," *Sens. Actuators B, Chem.*, vol. 200, pp. 235–244, Sep. 2014.

[18] S. L. Sharp, J. S. N. Paine, and J. D. Blotter, "Design of a linear ultrasonic piezoelectric motor," *J. Intell. Mater. Syst. Struct.*, vol. 21, no. 10, pp. 961–973, Jul. 2010.

[19] W.-H. Lee, C.-Y. Kang, D.-S. Paik, B.-K. Ju, and S.-J. Yoon, "Butterfly-shaped ultra slim piezoelectric ultrasonic linear motor," *Sens. Actuators A, Phys.*, vol. 168, no. 1, pp. 127–130, Jul. 2011.

[20] Z. Li, Z. Wang, P. Guo, L. Zhao, and Q. Wang, "A ball-type multi-DOF ultrasonic motor with three embedded traveling wave stators," *Sens. Actuators A, Phys.*, vol. 313, Oct. 2020, Art. no. 112161.

[21] S. Borodinas, P. Vasiljev, D. Mazeika, R. Bareikis, and Y. Yang, "Design optimization of double ring rotary type ultrasonic motor," *Sens. Actuators A, Phys.*, vol. 293, pp. 160–166, Jul. 2019.

[22] S. L. Zhou and Z. Y. Yao, "Design and optimization of a modal- independent linear ultrasonic motor," *IEEE Trans. Ultrason., Ferroelectr, Freq. Control*, vol. 61, no. 3, pp. 46–535, Mar. 2014.

[23] Z. Huang, S. Shi, W. Chen, L. Wang, L. Wu, and Y. Liu, "Development of a novel spherical stator multi-DOF ultrasonic motor using in-plane non-axisymmetric mode," *Mech. Syst. Signal Process.*, vol. 140, Jun. 2020, Art. no. 106658.

[24] X. Yang, Y. Liu, W. Chen, and J. Liu, "A cylindrical traveling wave ultrasonic motor using bonded-type composite beam," *Ultrasonics*, vol. 65, pp. 277–281, Feb. 2016.

[25] X. Xin, Y. Yu, J. Wu, X. Gao, Z. Li, X. Yi, W. Chen, and S. Dong, "A ring-shaped linear ultrasonic motor based on PSN-PMS-PZT ceramic," *Sens. Actuators A, Phys.*, vol. 309, Jul. 2020, Art. no. 112036.

[26] D. Lu, Q. Lin, B. Chen, C. Jiang, and X. Hu, "A single-modal linear ultrasonic motor based on multi vibration modes of PZT ceramics," *Ultrasonics*, vol. 107, Sep. 2020, Art. no. 106158.

[27] L. Zhou, Z. Yao, S. Dai, Y. He, and H. Xu, "Modeling and verification of life prediction of a V-shaped linear ultrasonic motor," *Rev. Sci. Instrum.*, vol. 92, no. 4, Apr. 2021, Art. no. 045003.

[28] J. Yan, Y. Liu, J. Liu, D. Xu, and W. Chen, "The design and experiment of a novel ultrasonic motor based on the combination of bending modes," *Ultrasonics*, vol. 71, pp. 205–210, Sep. 2016.

[29] H. Li, J. Deng, S. Zhang, H. Yu, and Y. Liu, "Design and experiment of a three-feet linear ultrasonic motor using third bending hybrid modes," *Sens. Actuators A, Phys.*, vol. 331, Nov. 2021, Art. no. 112990.

[30] S. Izuhara and T. Mashimo, "Design and characterization of a thin linear ultrasonic motor for miniature focus systems," *Sens. Actuators A, Phys.*, vol. 329, Oct. 2021, Art. no. 112797.

JIAN ZHANG received the B.S. and M.S. degrees in control theory and control engineering from the Liaoning University of Technology, China, in 2005 and 2008, respectively, and the Ph.D. degree in power electronics and power transmission from the Shenyang University of Technology, China, in 2022. He is currently a Professor with the School of Electrical Engineering, Yingkou Institute of Technology, China. His research interests include artificial intelligence and modern motion control, power electronics and power transmission, synchronous motor excitation system design and research, special motor design and control, and design and control of ultrasonic motor.

XIAOZHU WANG received the B.S. and M.S. degrees in mechanical design and theory from the Liaoning University of Technology, China, in 2005 and 2008, respectively. She is currently an Associate Professor with the School of Mechanical and Power Engineering, Yingkou Institute of Technology, China. Her research interests include mechanical design and theory, ultrasonic piezoelectric technology and theory, and design and control of ultrasonic motor.